IEEE Access
Multidisciplinary ⋮ Rapid Review ⋮ Open Access Journal

Received 5 August 2024, accepted 2 September 2024, date of publication 5 September 2024, date of current version 16 September 2024.

Digital Object Identifier 10.1109/ACCESS.2024.3454713

RESEARCH ARTICLE

Cylindrical Metasurface-Cladded Waveguide Filled With Positive- or Negative-Epsilon Dielectric

MIRKO MAGAROTTO, (Member, IEEE), LUCA SCHENATO, (Member, IEEE), MARCO SANTAGIUSTINA, (Member, IEEE), ANDREA GALTAROSSA, (Life Fellow, IEEE), AND ANTONIO-DANIELE CAPOBIANCO, (Member, IEEE)

Department of Information Engineering, University of Padova, 35131 Padua, Italy
National Inter-University Consortium for Telecommunications (CNIT), 43124 Parma, Italy

Corresponding author: Mirko Magarotto (mirko.magarotto@unipd.it)

This work was supported in part by the European Union under the Italian National Recovery and Resilience Plan (NRRP) of NextGenerationEU, partnership on "Telecommunications of the Future" through the program "RESTART" under Grant PE00000001; and in part by the Italian Ministry of University and Research (MUR) under Grant PRIN 2022 PNRR P2022RFF9K–FLAIRS.

ABSTRACT This work proposes a metasurface-cladded waveguide which may be filled with positive- or negative-epsilon materials. This design targets microwave plasma technology, particularly devices intended to be loaded with tenuous and dense plasma. Namely, the dielectric permittivity of the filling material is positive or negative, depending on the scenario. First, a theoretical model has been proposed to assess the electromagnetic propagation regime. Specifically, the cladding metasurface is treated as an anisotropic surface impedance imposed at the edge of the waveguide. Second, a possible design relying on a hollow dielectric substrate whose internal surface is coated with a lattice of metallic patches is numerically investigated. The results show that the waveguide propagates electromagnetic waves independently from the sign of the dielectric permittivity of the filling material. The latter parameter and the geometry of the metallic lattice are shown to be governing design parameters, in particular, in determining the cut-off frequency of the fundamental mode.

INDEX TERMS Metasurface-cladded waveguide, cylindrical waveguide, filled waveguide, negative-epsilon, microwave plasma.

I. INTRODUCTION

Plasma is usually referred to as the fourth state of matter. It is an ionized gas composed of positively and negatively charged particles [1]. Microwave plasma is a widespread technology that finds application in several fields [2]. Examples worth to be mentioned are material etching [3], electric space propulsion [4], [5], and plasma antennas [6]. The solutions most frequently adopted to generate plasma relying on microwave power are surface wave [7] and electron cyclotron resonance [8] discharges. Microwave systems, yet mature enough, are still susceptible to the typical issues encountered in plasma discharges. These include the need for a power budget to sustain the plasma and the challenge of impedance matching due to the variable load presented by the plasma [9], [10]. Moreover, from an electromagnetic (EM) perspective, plasma is a peculiar medium whose dielectric permittivity can assume both positive and negative values [11].

Plasma-loaded waveguides have been a topic of research since the 1960s [12]. Most wave-driven plasma discharges can be modeled as segments of waveguides filled with either non-magnetized (isotropic) [13] or magnetized (anisotropic) [14] plasma. Extensive experimental work has been done to investigate EM plasma propagation in the framework of material processing [15], space propulsion [4], and plasma antennas [16]. Additionally, numerous theoretical studies on plasma-loaded waveguides have been published

The associate editor coordinating the review of this manuscript and approving it for publication was Wanchen Yang.

since the 1960s. These studies include the analysis of plasma layers in free space [12] and those confined by conductive walls [17]. Both non-magnetized [18] and magnetized [19] configurations have been considered. To address more realistic, non-uniform plasma configurations, numerical models have been developed for both plane [20], [21] and cylindrical [22], [23] geometries. Other significant works include the analysis of guided and leaky wave modes in magnetized plasma layers [24], [25].

The EM propagation in waveguides filled with unconventional materials has attracted researchers over the last decades. The propagation in waveguides lined with epsilon-negative, mu-negative, or double-negative materials has been assessed in several works, including cylindrical [26], and parallel-plate geometries [27]. These configurations enable below-cutoff propagation, field collimation, and miniaturization [28], [29]. Notably, a proof-of-concept implemented in cylindrical geometry has been assessed in [30]. Similar analyses are performed for rectangular [31], [32] and cylindrical [33] waveguides loaded with metamaterials.

Recently, the adoption of cladding-metasurfaces has been proposed to modify the propagation in waveguides [34]. Specifically, metasurfaces are a technology that allows controlling the EM fields tangential to the surface [35]. This, in turn, enables achieving epsilon-negative and mu-negative behavior [36] or surface waves propagation [37]. Metasurfaces are adopted in waveguides to control cut-off, enhance field confinement for electromagnetic bandgap, and break the degeneracy of left-handed and right-handed wave modes [38]. Theoretically, cladding-metasurfaces can be treated as sub-wavelength thin layers whose properties are derived from the bulk material parameters [39]. The corresponding constitutive relation can be translated into generalized sheet boundary conditions. Thus, they can be interpreted as liners that transition the Perfect Electric Conductor (PEC) condition imposed in conventional waveguides to an effective surface impedance [40]. This methodology has been adopted to handle rectangular [41] and cylindrical [42] geometries. Notably, proofs of concepts that exploit cladding-metasurfaces in rectangular waveguides are proposed in literature [43], [44].

This work focuses on EM propagation in cylindrical metasurface-cladded waveguides loaded with generic dielectric material. The proposed device allows EM waves to propagate in the presence of either tenuous or dense plasma, resulting in a dielectric permittivity that is either positive or negative [11]. This capability is crucial for designing efficient plasma discharges or waveguides that interface the actual source with the microwave power unit [2]. Additionally, a metasurface-cladded waveguide can function as a plasma diagnostic system [45], as waveguides are commonly used in sensing applications where wave modes are sensitive to the local dielectric environment [46]. While EM propagation in cylindrical waveguides filled with plasma has been extensively analyzed [47], [48], to the best of the authors' knowledge, this is the first study to propose using a metasurface to line a plasma-loaded waveguide. Moreover, the proposed metasurface-cladded waveguide can be loaded with both conventional and epsilon-negative materials, advancing the current literature, which only addresses metasurface-cladded waveguides filled with positive-epsilon dielectrics [49].

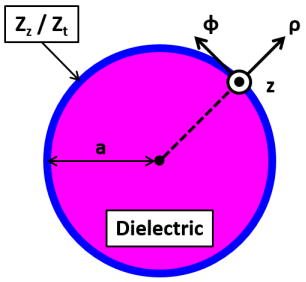

FIGURE 1. Scheme of the theoretical model.

II. METHODOLOGY

A. THEORETICAL MODEL

The EM propagation within a metasurface-cladded waveguide is studied, introducing the equivalent system depicted in Fig. 1 [34], [40], [42]. A cylinder of radius a and infinite axial extension is filled with a dielectric material of relative permittivity ε_r. It is lined with a sheet of negligible thickness that presents an anisotropic surface impedance (Z_t, Z_z) [34]. The sheet approximates the cladding metasurface and is introduced, without loss of generality, to simplify the analytical solutions of the problem at hand [40], [42]. Assuming a dependence from time and space in the form $\exp[\jmath(\omega t - \beta z \pm m\phi)]$, Maxwell's equations are solved in the cylindrical reference frame (ρ, ϕ, z) [50, Chap. 3.4] [51, Chap. 5.3] [52] where ω is the angular frequency, β the axial wavenumber, and m the azimuthal wavenumber. In particular, m is a positive integer, and the sign $\pm$ determines if the propagation is right-handed or left-handed [38]. Consistently with the results presented in [53] and [54], the EM fields for $\rho \leq a$ read

$$E_z = E_0 \frac{I_m(\tau\rho)}{I_m(\tau a)}, \tag{1}$$

$$E_\rho = E_0 \left[\jmath \frac{\beta}{\tau} \frac{I'_m(\tau\rho)}{I_m(\tau a)} \mp \frac{\eta_0 H_0}{E_0} \frac{m}{\tau\rho} \frac{k_0}{\tau} \frac{I_m(\tau\rho)}{I_m(\tau a)} \right], \tag{2}$$

$$H_\phi = \frac{E_0}{\eta_0} \left[\jmath \frac{\varepsilon_r k_0}{\tau} \frac{I'_m(\tau\rho)}{I_m(\tau a)} \mp \frac{\eta_0 H_0}{E_0} \frac{m}{\tau\rho} \frac{\beta}{\tau} \frac{I_m(\tau\rho)}{I_m(\tau a)} \right], \tag{3}$$

$$H_z = H_0 \frac{I_m(\tau\rho)}{I_m(\tau a)}, \tag{4}$$

$$H_\rho = H_0 \left[\jmath \frac{\beta}{\tau} \frac{I'_m(\tau\rho)}{I_m(\tau a)} \pm \frac{E_0}{\eta_0 H_0} \frac{m}{\tau\rho} \frac{\varepsilon_r k_0}{\tau} \frac{I_m(\tau\rho)}{I_m(\tau a)} \right], \tag{5}$$

$$E_\phi = \eta_0 H_0 \left[-\jmath \frac{k_0}{\tau} \frac{I'_m(\tau\rho)}{I_m(\tau a)} \mp \frac{E_0}{\eta_0 H_0} \frac{m}{\tau\rho} \frac{\beta}{\tau} \frac{I_m(\tau\rho)}{I_m(\tau a)} \right], \tag{6}$$

where η_0 is the impedance of free space, $k_0 = \omega/c_0$ is the wavenumber in vacuum, and c_0 is the speed of light. E_0 and H_0 are complex constants in V/m and A/m, respectively.

I_m indicates the modified Bessel function of the first kind and order m. The parameter τ is equivalent to the transverse wavenumber and reads

$$\tau = \sqrt{\beta^2 - \varepsilon_r k_0^2}\,. \tag{7}$$

It is worth noting that the EM fields in Eqs. 1–6 are expressed using the modified Bessel functions I_m [51, Chap. 5.3], rather than the Bessel functions J_m typically adopted for cylindrical waveguides [50, Chap. 3.4]. Although both formalisms yield equivalent results, the modified Bessel functions are used because they are more suitable for describing the surface waves that propagate in metasurface-cladded waveguides [39] and waveguides filled with negative-epsilon materials [13].

To determine the dispersion relation of the waveguide, the following boundary conditions are imposed [34]

$$Z_t = \left.\frac{E_\phi}{H_z}\right|_{\rho=a}, \tag{8}$$

$$Z_z = -\left.\frac{E_z}{H_\phi}\right|_{\rho=a}, \tag{9}$$

where Z_t and Z_z are the transverse and axial surface impedance, respectively. Relying on the expressions reported in Eqs. 1-6, the following dispersion relation is obtained solving simultaneously Eq. 8 and Eq. 9:

$$0 = \left(\frac{m}{\tau a}\frac{\beta}{\tau}\right)^2 + \left(\jmath\frac{k_0}{\tau}\frac{I_m'(\tau a)}{I_m(\tau a)} + \frac{Z_t}{\eta_0}\right)\left(\jmath\frac{\varepsilon_r k_0}{\tau}\frac{I_m'(\tau a)}{I_m(\tau a)} + \frac{\eta_0}{Z_z}\right). \tag{10}$$

Specifically, the axial wavenumber can be computed once the adimensional parameters m, ε_r, $k_0 a$, Z_t/η_0, and Z_z/η_0 are fixed. Notably, a second condition follows from the solution of Eqs. 8, 9:

$$\pm\frac{E_0}{\eta_0 H_0} = -\left(\frac{\tau a}{m}\frac{\tau}{\beta}\right)\left(\jmath\frac{k_0}{\tau}\frac{I_m'(\tau a)}{I_m(\tau a)} + \frac{Z_t}{\eta_0}\right), \tag{11}$$

or alternatively

$$\pm\frac{\eta_0 H_0}{E_0} = \left(\frac{\tau a}{m}\frac{\tau}{\beta}\right)\left(\jmath\frac{\varepsilon_r k_0}{\tau}\frac{I_m'(\tau a)}{I_m(\tau a)} + \frac{\eta_0}{Z_z}\right). \tag{12}$$

Thus, the modes associated with right-handed and left-handed propagation are degenerate, given that any ambiguity between signs can be removed by introducing Eq. 11 or Eq. 12 in Eqs. 1-6 [38]. More interestingly, in a metasurface-cladded waveguide, it is impossible to separate TE and TM modes given that the coefficients E_0 and H_0 are not independent of one another [55], [56], [57]. Specifically, a similar-TE propagation is associated with the condition $|\eta_0 H_0/E_0| \gtrsim 1$ and is referred to as HE mode, otherwise the hybrid mode is similar-TM and is called EH [55], [56], [57]. The only case in which TE and TM modes are independent is for $m = 0$ [39].

In that case, the dispersion relation reduces to

$$Z_t = -\jmath\eta_0\frac{k_0}{\tau}\frac{I_1(\tau a)}{I_0(\tau a)} \quad \text{TE}_{01}\text{ mode}\,, \tag{13}$$

$$Z_z = \jmath\eta_0\frac{\tau}{\varepsilon_r k_0}\frac{I_0(\tau a)}{I_1(\tau a)} \quad \text{TM}_{01}\text{ mode}\,. \tag{14}$$

Notably, the expression reported in Eq. 14 is fully consistent with the results presented in [39].

Manipulating Eq. 10, it is possible to prove that cut-off, namely $\beta = 0$ [50, Chap. 3.4], occurs if one of the following conditions is matched

$$Z_t^c = \eta_0\frac{\jmath}{\sqrt{\varepsilon_r}}\frac{J_m'(\sqrt{\varepsilon_r}k_0 a)}{J_m(\sqrt{\varepsilon_r}k_0 a)} \quad \text{HE modes}\,, \tag{15}$$

$$Z_z^c = -\eta_0\frac{\jmath}{\sqrt{\varepsilon_r}}\frac{J_m(\sqrt{\varepsilon_r}k_0 a)}{J_m'(\sqrt{\varepsilon_r}k_0 a)} \quad \text{EH modes}\,, \tag{16}$$

The cut-off condition associated with HE modes is given in Eq. 15 since using the expression of Z_t^c in Eq. 11 results in $|E_0/\eta_0 H_0| \to 0$. Vice versa, Eq. 16 refers to EH modes [26], [28]. Eqs. 15, 16 also provide a second preliminary verification of the theoretical model for $Z_t^c = Z_z^c = 0$, namely if the cladding metasurface is a sheet of Perfect Electric Conductor (PEC) [34]. In this case, the cut-off conditions expressed in Eqs. 15, 16 match perfectly the ones derived via the standard solution of cylindrical metallic waveguides [50, Chap. 3.4]. Moreover, the electric field parallel to the cladding metasurface and the magnetic field perpendicular to it are null for $\rho = a$.

Finally, it is worth mentioning that the proposed theoretical model can handle a generic expression for ε_r. In the case of a plasma medium, which represents the main target of this work, the relative dielectric permittivity reads

$$\varepsilon_r = 1 - \frac{\omega_p^2}{\omega(\omega - \jmath\nu_c)}\,, \tag{17}$$

where ω_p, evaluated in rad/s, is the plasma frequency and ν_c, evaluated in Hz, is the collision frequency. Notably, $\text{Re}(\varepsilon_r) \geq 0$ for $\omega \geq \omega_p$, otherwise plasma is an epsilon-negative material [11].

B. NUMERICAL MODEL

The commercial software CST Studio Suite ®has been exploited to simulate the EM propagation in the metasurface-cladded waveguide. Maxwell's equations are solved in the frequency domain, relying on an unstructured tetrahedral mesh and imposing open boundary conditions [39]. The signal is coupled to the waveguide via a PEC ring excited through a discrete face port [28]. The design depicted in Fig. 2 is numerically investigated to validate the theoretical model. In the scheme, the material labeled "Dielectric" is assumed to have a relative dielectric permittivity ε_r. An isotropic surface impedance is imposed at the edge of the waveguide assigning the native CST material named "Surface Impedance" to the cladding. Since CST only allows for isotropic surface impedance, the theoretical model is verified for $Z_t = Z_z$ in Section III.

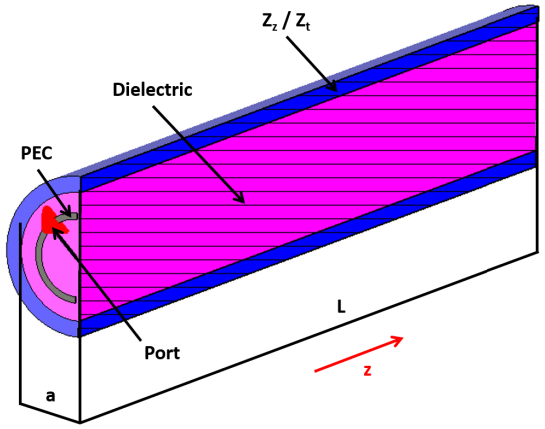

FIGURE 2. Axial cross-section of the numerical model used to verify the theoretical model.

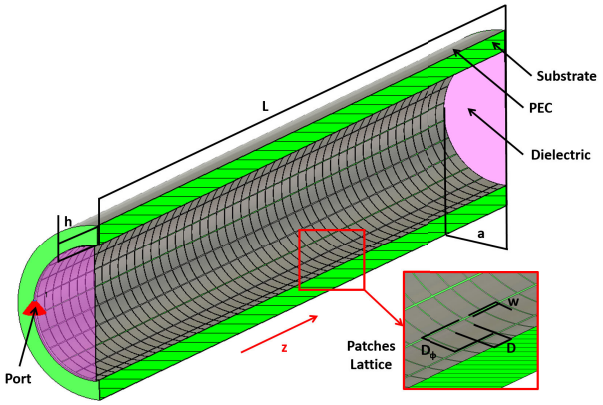

FIGURE 3. Axial cross-section of the proposed metasurface-cladded waveguide.

On the other hand, Fig. 3 shows a realistic implementation of a metasurface-cladded waveguide. Here, the surface impedance is not predetermined but results from the metasurface design [44], [58]. The inner side of the dielectric "Substrate" is coated with a lattice of metallic patches. By tuning the dimensions of each patch, the equivalent surface impedance that governs EM propagation within the waveguide can be controlled [59]. Specifically, cases resulting in an anisotropic surface impedance are analyzed in Section IV, providing further verification of the theoretical model. Finally, the entire waveguide is enclosed within a cylindrical metallic sheet for confinement.

III. THEORETICAL ANALYSIS

The theoretical model is exploited to assess the EM propagation in the metasurface-cladded waveguide introduced in section II. For simplicity's sake, losses of the wall and the dielectric material are neglected; this corresponds to having a purely imaginary surface impedance and a real ε_r [34]. This assumption is further delved into Appendix A.

A. DIELECTRIC PERMITTIVITY

The proposed design targets materials with positive or negative values of ε_r. Thus, the dispersion relation in Eq. 10

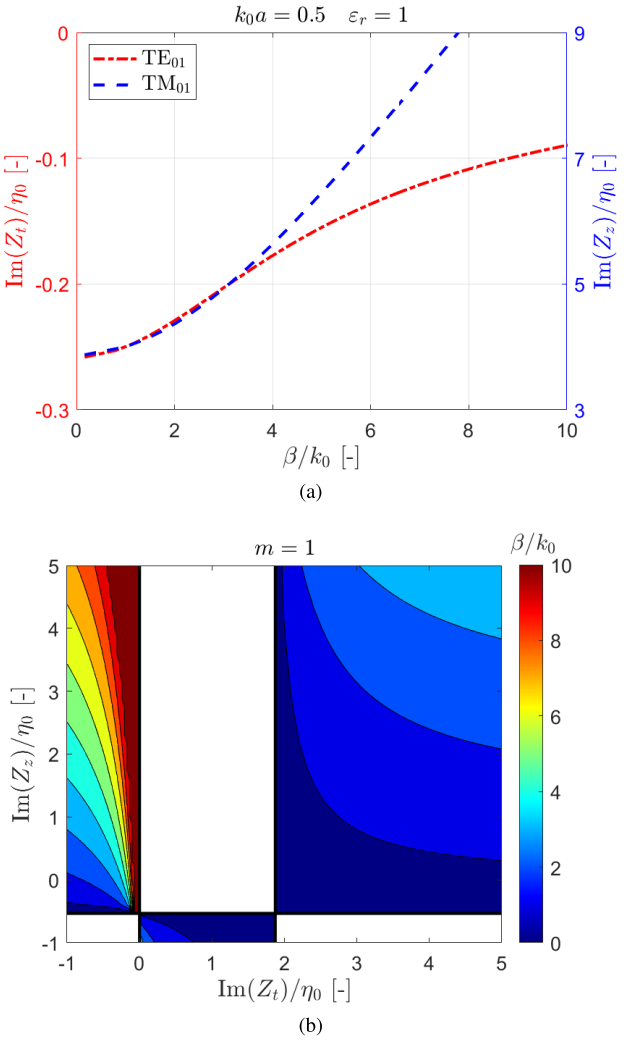

FIGURE 4. Normalized axial wavenumber β/k_0 vs. surface impedance for $k_0a = 0.5$, $\varepsilon_r = 1$, and (a) $m = 0$, or (b) $m = 1$.

is solved for $\varepsilon_r = 1$ and $\varepsilon_r = -1$; results are reported in Fig. 4 and Fig. 5, respectively. The waveguide analyzed is electromagnetically "small" being $k_0a = 0.5$ as, in a metallic cylindrical waveguide, propagation is possible only for $k_0a \geq 1.841$ [50, Chap. 3.4].

In the case of $\varepsilon_r = 1$, the mode TE$_{01}$ propagates for negative values of $\mathrm{Im}(Z_t)$, in particular $Z_t^c \leq Z_t \leq 0$ [42]. Instead, the mode TM$_{01}$ is associated to positive values of $\mathrm{Im}(Z_z)$, specifically $Z_z \geq Z_z^c$ [39]. Notably, in a system in which Z_t and Z_z can be controlled separately, the two modes associated with $m = 0$ are independent. If $m = 1$ the combinations of Z_t and Z_z enabling propagation are less trivial [34], [40]. Specifically, the cut-off condition occurs in correspondence of Z_t^c and Z_z^c while, in "small" waveguides, a resonance is encountered for $Z_t = 0$ (i.e., $\beta \to \infty$) [32]. Notably, the trend followed by higher order hybrid modes (i.e., $m \geq 2$) is similar to one for $m = 1$ as long as the cut-off conditions prescribed in Eqs. 15, 16 are considered.

If $\varepsilon_r = -1$, the behavior of the TE$_{01}$ mode is almost unchanged with respect to the case $\varepsilon_r = 1$. The situation

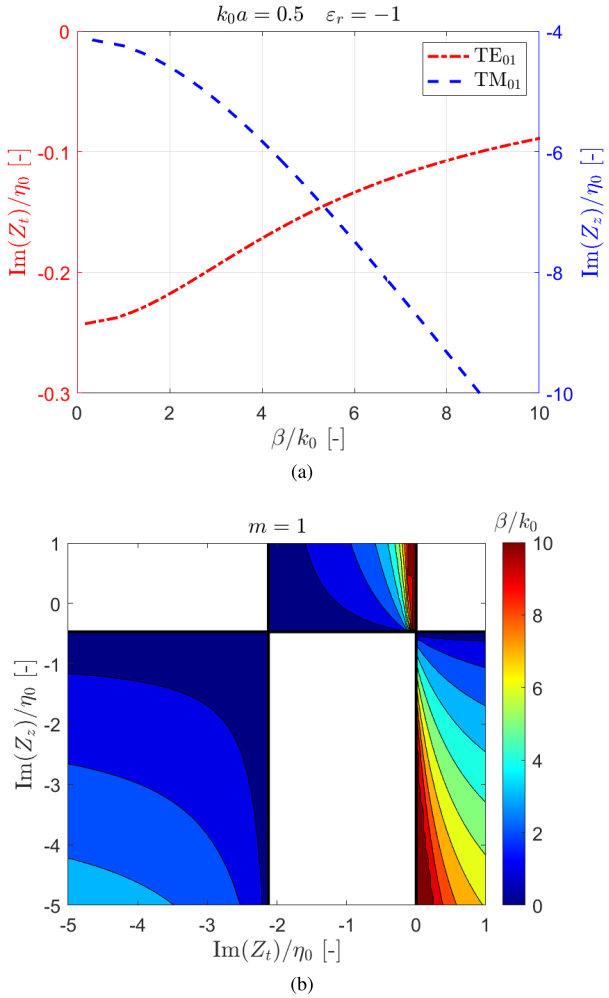

FIGURE 5. Normalized axial wavenumber β/k_0 vs. surface impedance for $k_0a = 0.5$, $\varepsilon_r = -1$, and (a) $m = 0$, or (b) $m = 1$.

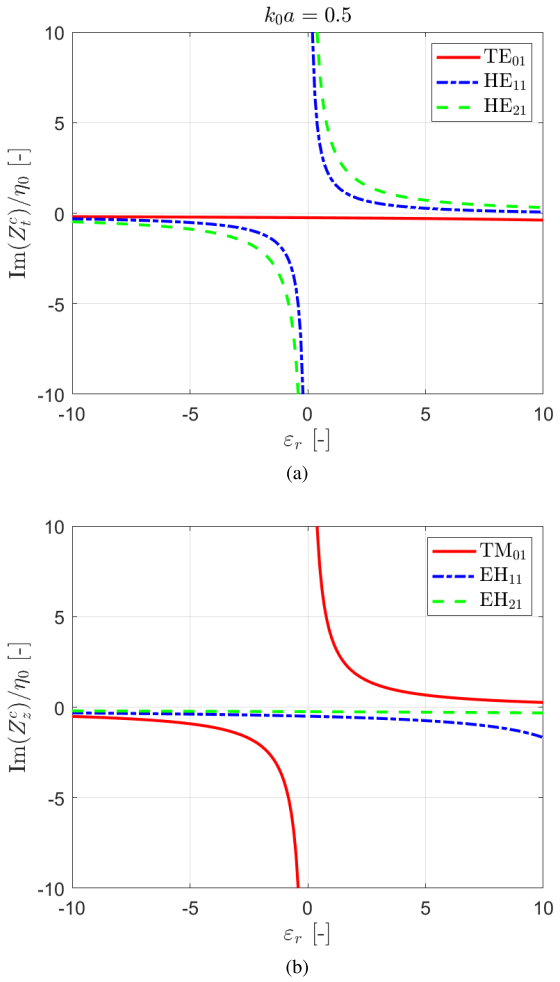

FIGURE 6. (a) Transversal, and (b) axial threshold surface impedance to stimulate modes $m = 0, 1, 2$ vs. dielectric permittivity ε_r.

is different for the TM_{01} mode given that negative values of $\mathrm{Im}(Z_z)$ are required and, in particular, $Z_z \leq Z_z^c$. Nevertheless, with $\varepsilon_r < 0$, the wave modes associated with $m = 0$ are independent. Relying on suitable combinations of Z_t and Z_z, the propagation of hybrid modes for $m = 1$ is also possible. Specifically, the resonance condition for $Z_t = 0$ still holds, and the value of Z_z^c is almost the same as the case $\varepsilon_r = 1$; on the contrary, Z_t^c changes sign. Similar considerations hold for higher-order hybrid modes.

The trends reported in Figs. 4, 5 can be explained in different ways. First, for $\varepsilon_r = 1$ and $\beta \leq k_0$ (i.e., Fig. 4), waves propagate obliquely with respect to the axis of the system, similarly to what happens in metallic cylindrical waveguides [50, Chap. 3.2]. Given that the boundary conditions do not necessitate the fields being null at the edge of the waveguide, the cut-off conditions change consequently [38]. For $\varepsilon_r = 1$ and $\beta > k_0$, instead, it is helpful to consider the equivalence between a surface impedance sheet and the discontinuity among different materials [39]. Specifically, the EM propagation regime, in this case, is equivalent to a surface wave occurring at the interface between the inner cylinder and a fictitious background characterized by a negative dielectric permittivity [39]. Similarly, for $\varepsilon_r = -1$, the same equivalence still holds. In fact, the possibility of stimulating surface waves within plasma columns ($\varepsilon_r < 0$) immersed in air is well known [7], [60]. Thus, for $\varepsilon_r = -1$, an adequately selected surface impedance allows the propagation of EM signals equivalent to the surface waves mentioned above.

Fig. 6 depicts the cut-off conditions Z_t^c and Z_z^c to provide a clearer picture of how ε_r affects the EM propagation. Specifically, only the TE_{01} mode is not significantly affected by ε_r. On the contrary, Z_z^c related to TM_{01} shows an almost inverse proportionality with ε_r. The same occurs in HE hybrid modes for which Z_t^c is concerned. At the same time, Z_z^c is not particularly affected by ε_r if $m \geq 1$. Finally, the resonance condition occurring at $Z_t = 0$ in electromagnetically "small" waveguides does not depend straightly on ε_r.

B. FREQUENCY ANALYSIS

The frequency response is a crucial design parameter of a waveguide. Fig. 7 shows the normalized axial wavenumber β/k_0 as a function of the normalized propagation constant k_0a

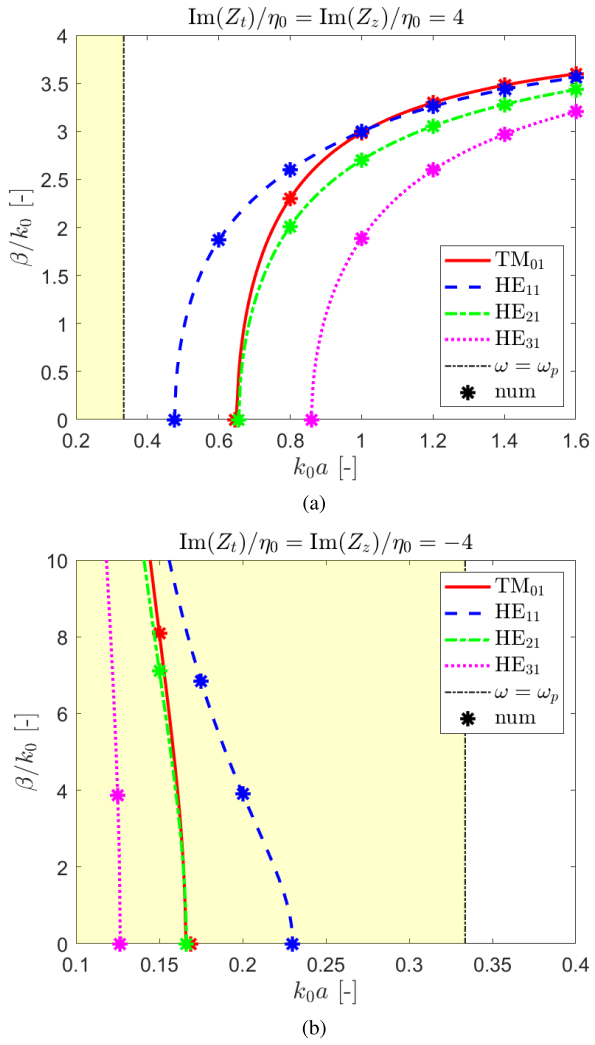

FIGURE 7. Dispersion relation for the modes $m = 0, 1, 2, 3$: (a) positive and (b) negative arbitrary surface impedance. Plasma medium is considered such that $a\omega_p/c_0 = 0.33$. Yellow background indicates $\omega < \omega_p$. Theoretical (continuous and dashed lines) and numerical ("num") models are compared.

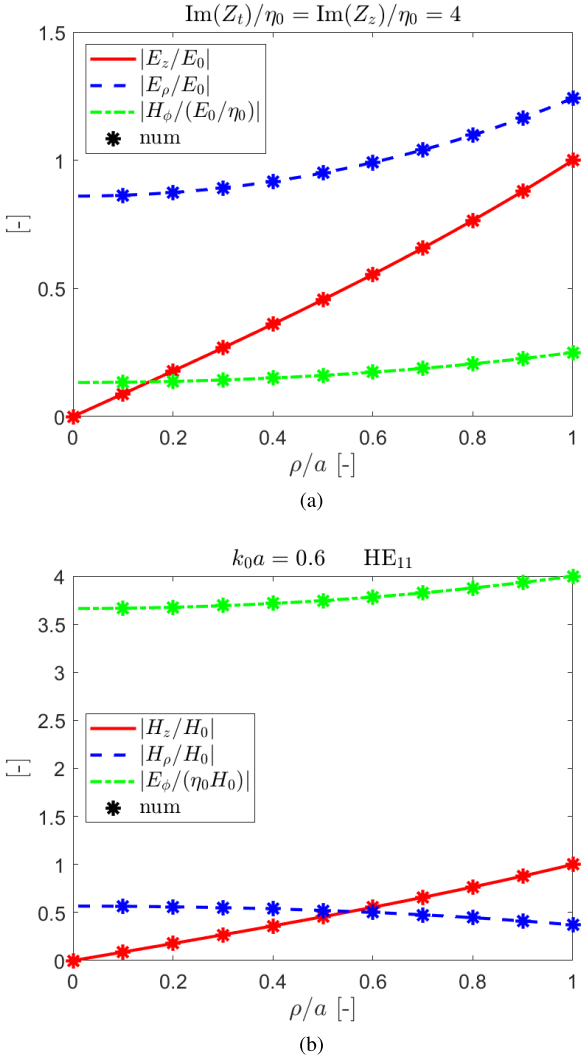

FIGURE 8. Normalized EM fields vs. normalized radial coordinate ρ/a. Same conditions as in Fig 7. The results of the theoretical (continuous and dashed lines) and numerical ("num") models are compared.

(proportional to the signal frequency, as $k_0 = 2\pi f/c_0$). Given the dispersive nature of the plasma medium, it is worth performing this analysis considering ε_r as prescribed by Eq. 17 rather than fixing its value. Specifically, ω_p is defined via an adimensional parameter that reads $\omega_p a/c_0 = 0.33$ while arbitrary pairs of Z_t and Z_z are assumed. Notably, the propagation associated with positive values of the surface impedance requires $\varepsilon_r > 0$ being $\omega > \omega_p$. Vice versa, the condition $\varepsilon_r < 0$ holds if the surface impedance is negative. This is coherent with the qualitative wave dynamics described in Section III-A. Moreover, the fundamental mode is HE$_{11}$ regardless of the sign of the surface impedance consistently with the inverse proportionality identified in Fig. 6 between ε_r and the cut-off impedance for the TM$_{01}$ and HE modes. In the case with positive surface impedance, the only mode that propagates at $k_0a = 0.6$ is HE$_{11}$ (see Fig. 7a). The EM fields evaluated in this condition are depicted in Fig. 8. Consistently with the results presented in [39], a metasurface-cladded waveguide can be designed to maximize the intensity of the fields on the system's edge rather than its axis because of the propagation of surface waves.

Notably, the theoretical results depicted in Figs. 7, 8 are verified against numerical estimations obtained using the setup depicted in Fig. 2. The numerical simulations assume $a = 10$ mm, $\omega_p = 10^{10}$ rad/s, and $L = 200$ mm. The frequency is varied in the range 0.5–5 GHz, with the specific comparison in Fig. 8 obtained for $f = 2.86$ GHz. Theoretical and numerical results are in close agreement. The axial wavenumber is evaluated by applying a Fourier transform to the computed fields along the z-axis [39], revealing a negligible discrepancy of less than 1% between theoretical and numerical calculations. A similar agreement is obtained for the EM fields, as shown in Fig. 8. This constitutes a

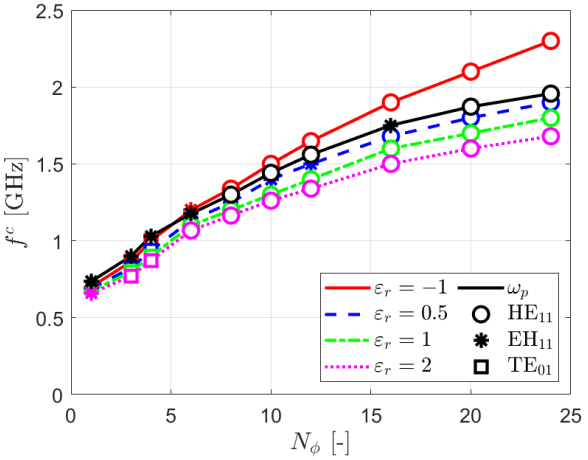

FIGURE 9. Cut-off frequency vs. number of azimuthal patches N_ϕ for different values of the dielectric permittivity ε_r. The label ω_p identifies a dispersive plasma where $\omega_p = 10^{10}$ rad/s. Markers indicate the fundamental mode.

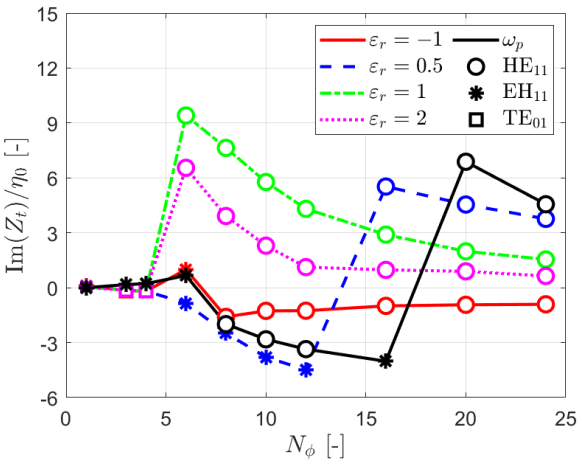

FIGURE 10. Transverse surface impedance vs. number of azimuthal patches N_ϕ for different values of ε_r. The label ω_p identifies a dispersive plasma where $\omega_p = 10^{10}$ rad/s. Markers indicate the fundamental mode.

TABLE 1. Dielectric permittivity ε_r at the cut-off for $\omega_p = 10^{10}$ rad/s.

N_ϕ	f^c [GHz]	ε_r
1	0.7	−4.1
3	0.9	−2.1
4	1.0	−1.5
6	1.1	−0.8
8	1.2	−0.5
10	1.3	−0.3
12	1.4	−0.1
16	1.6	0.1
20	1.7	0.2
24	1.8	0.3

verification of the theoretical model for an isotropic surface impedance.

IV. NUMERICAL ANALYSIS

The design of the proposed metasurface-cladded waveguide is depicted in Fig. 3. Specifically, the internal radius is $a = 20$ mm, and the thickness of the substrate is $h = 6$ mm. The substrate material is a dielectric with relative permittivity $\varepsilon_s = 10$ (e.g., RT/duroid ® [61]). The internal side of the waveguide is "coated" with a lattice of metallic patches whose periodicity in the z-direction is $D = \pi a/12 = 5.2$ mm. The simulated waveguide comprises 50 rings of metallic patches in the axial direction, namely $L = 262$ mm. Along the azimuthal ϕ-direction, each patch is long $D_\phi \approx 2\pi a/N_\phi$, where the integer N_ϕ represents the number of metallic elements on each ring and varies from 1 to 24. For example, Fig. 3 corresponds to $N_\phi = 24$ square patches with $D_\phi = D$. Instead, when $N_\phi = 1$, the lattice is made of uniform annuli [40]. Adjacent patches are separated from one another by $w = 0.3$ mm. The waveguide is filled with a uniform material with relative permittivity ε_r that can assume both arbitrary fixed values or follow the disperse behavior prescribed by Eq.17 when $\omega_p = 10^{10}$ rad/s.

A. CUT-OFF ANALYSIS

Fig. 9 represents the cut-off frequency f^c for different values of ε_r and N_ϕ. The cut-off is first analyzed for fixed ε_r. Subsequently, the dispersive nature of the plasma is taken into account to prove that the dynamics of the system depend on the actual value of ε_r. For a given filling material, the cut-off frequency increases with N_ϕ. Interestingly, for $N_\phi = 1$ and $\varepsilon_r = 1$ the cut-off frequency is $f^c = 0.7$ GHz. In a cylindrical metallic waveguide with comparable external radius (i.e., $a + h = 26$ mm), the cut-off frequency is way larger, namely $f^c = 3.4$ GHz [50, Chap. 3.4]. As expected, f^c decreases for larger values of ε_r. Again, for metallic waveguides $f^c \propto 1/\sqrt{\varepsilon_r}$ while for the system at hand, the dependence of f^c from ε_r is weaker. More notably, the same structure can support EM propagation if the filling dielectric has, indifferently, positive or negative dielectric permittivity. This property is extremely appealing to design plasma sources in which EM waves propagate both in case of tenuous ($\varepsilon_r > 0$) or dense ($\varepsilon_r < 0$) plasma [11]. Lastly, N_ϕ determines also the fundamental mode of the waveguide. Regardless of the value of ε_r, the fundamental mode is associated with $m = 1$ unless for $N_\phi = 3, 4$ where it can be replaced by TE_{01}.

Fig. 10 depicts the transverse surface impedance Z_t computed at the cut-off. Analyzing the surface impedance is key to determining the cut-off dynamics since a mode exists at a certain frequency only if Z_t and Z_z are compatible with its propagation (e.g., see Figs. 4, 5). Nonetheless, when handling a realistic cladding metasurface, Z_t and Z_z are unknown a-priori [44]. In this work, they are estimated to satisfy the dispersion relation Eq. 10, where β is computed Fourier transforming results along the z-axis [39], and to fit the EM fields propagating within the waveguide at best. As shown in Section IV-B, this procedure, which relies on the least square method [39], allows to reproduce the actual EM fields with errors below a few percent points. In general, if the fundamental mode is HE_{11}, $\mathrm{Im}(Z_t^c)$ is expected to have the

same sign as ε_r. While the condition $\mathrm{Im}(Z_z^c) < 0$ holds if the fundamental model is EH_{11} (see Fig. 6). Namely, if the number of metallic patches is sufficiently high, cut-off occurs since Z_t follows the trend prescribed for Z_t^c (see the circle markers in Fig. 10). Vice versa, the cut-off is driven by negative Z_z values that follow the trend of Z_z^c. When the fundamental mode is TE_{01}, $\mathrm{Im}(Z_t^c) < 0$.

If $N_\phi \geq 6$, the trend of Z_t can be qualitatively explained by relying on a simplified analytical model of plane metasurfaces [37], [59], [62], [63]. The cut-off frequency is the one that allows the surface impedance to meet the conditions expressed in Eqs. 15, 16 [26], [28]. Specifically, the filling material affects the cut-off impedance Z_t^c and Z_z^c (see Fig. 6) while the geometry of the patches has a major effect on the actual surface impedance Z_t and Z_z [37]; see Appendix B for further details. Specifically, the value of N_ϕ, and in turn of D_ϕ, can produce an inversion of the sign of the surface impedance [37] with two important consequences. First, the EM propagation is possible regardless of the value of ε_r since cut-off conditions with opposite signs can be matched by adjusting N_ϕ and f. Second, N_ϕ can produce a sign inversion in Z_t [39]. If so, the only option to meet the cut-off conditions is ensuring a negative value of $\mathrm{Im}(Z_z)$ that matches Z_z^c. As a result, the fundamental mode changes from HE_{11} to EH_{11}.

On the other hand, if $N_\phi \leq 4$, it is necessary to consider that the cladding metasurface is a conformal structure whose behavior departs from planar geometries [64]. Specifically, $Z_t \to 0$ as in a metallic waveguide since $D_\phi \approx a$ and, thus, the homogenization of the lattice is no more consistent [65], [66]. The fundamental mode for $N_\phi = 1$ is EH_{11}, consistently with [34] and [40]. Namely, the cut-off frequency is determined by Z_z^c being $\mathrm{Im}(Z_z) < 0$. On the other hand, if the fundamental mode is TE_{01}, then $\mathrm{Im}(Z_t) < 0$ and whatever value of Z_z is acceptable. In summary, it is not surprising that in certain conditions, TE_{01} is triggered at lower frequencies than HE_{11} or EH_{11} given that the fundamental mode depends on the ratio between Z_t and Z_z and, in turn, on the geometry of the waveguide [34].

Finally, if a realistic plasma is considered, the dynamics of the system depend on the actual value of ε_r reported in Table 1. A notable features is registered for $N_\phi = 16$ since $\varepsilon_r > 0$ but the metasurface imposes $\mathrm{Im}(Z_t) < 0$, namely the fundamental mode is EH_{11} in spite being HE_{11} for $N_\phi = 12$ and $N_\phi = 20$. At the same time, the fundamental mode for $N_\phi = 3, 4$ is EH_{11} and not TE_{01}. This discrepancy with respect to fixed ε_r cases can be attributed to $\varepsilon_r < -1$.

B. EM FIELDS

Finally, the EM fields are analyzed to verify that the propagation in the metasurface-cladded waveguide aligns with theoretical predictions for a generic, not just isotropic, surface impedance. Specifically, as outlined in Section IV-A, Z_t and Z_z arise from the design of the waveguide and are not predetermined. They are calculated to satisfy the dispersion relation in Eq. 10 and to best fit the EM field profiles. The first condition establishes a one-to-one relationship between Z_t and Z_z based on the system's geometry, the operation frequency, and the value of β, which is determined by Fourier transforming the EM field maps along the z-axis. Subsequently, the least square method is used to determine the pair (Z_t, Z_z) that best fits the EM field profiles. Therefore, using CST, the only way to verify the theoretical formulation for an anisotropic surface impedance is by comparing the numerically evaluated EM field profiles with those derived from the best-fitting pair (Z_t, Z_z). To this end, the case $N_\phi = 24$ has been considered. Numerical and theoretical results are compared in Fig. 11 for $\varepsilon_r = 1$, and in Fig. 12 for $\varepsilon_r = -1$. Specifically, the modulus of the radial electric field E_ρ is represented in the axial cross-section of the waveguide; colored arrows represent the vector (E_ρ, E_z). Notably, theoretical and numerical predictions match well unless in proximity to the cladding metasurface. Such discrepancy is expected since homogenization fails

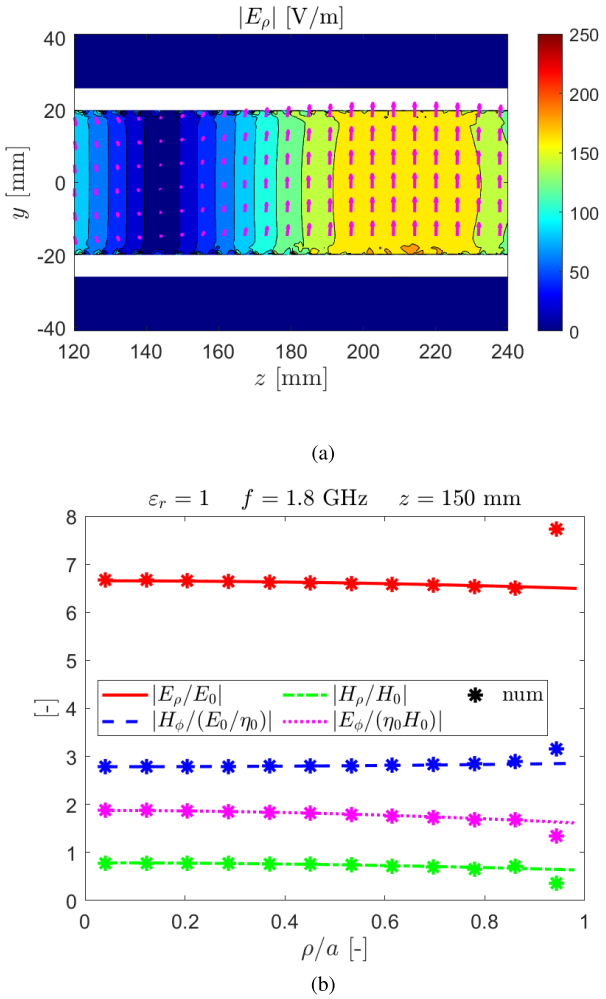

FIGURE 11. a) The electric field in the axial cross-section, and (b) a comparison between the numerical and theoretical estimations of the normalized EM fields at $z = 150$ mm. $f = 1.8$ GHz is close to cut-off for $N_\phi = 24$ and $\varepsilon_r = 1$.

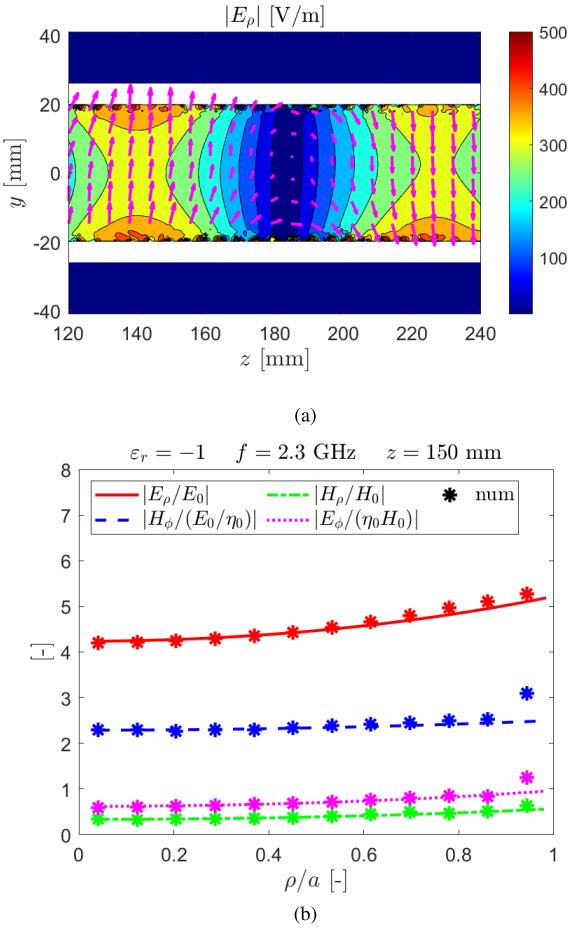

FIGURE 12. (a) The electric field in the axial cross-section, and (b) a comparison between the numerical and theoretical estimations of the normalized EM fields at $z = 150$ mm. $f = 2.3$ GHz is close to cut-off for $N_\phi = 24$ and $\varepsilon_r = -1$.

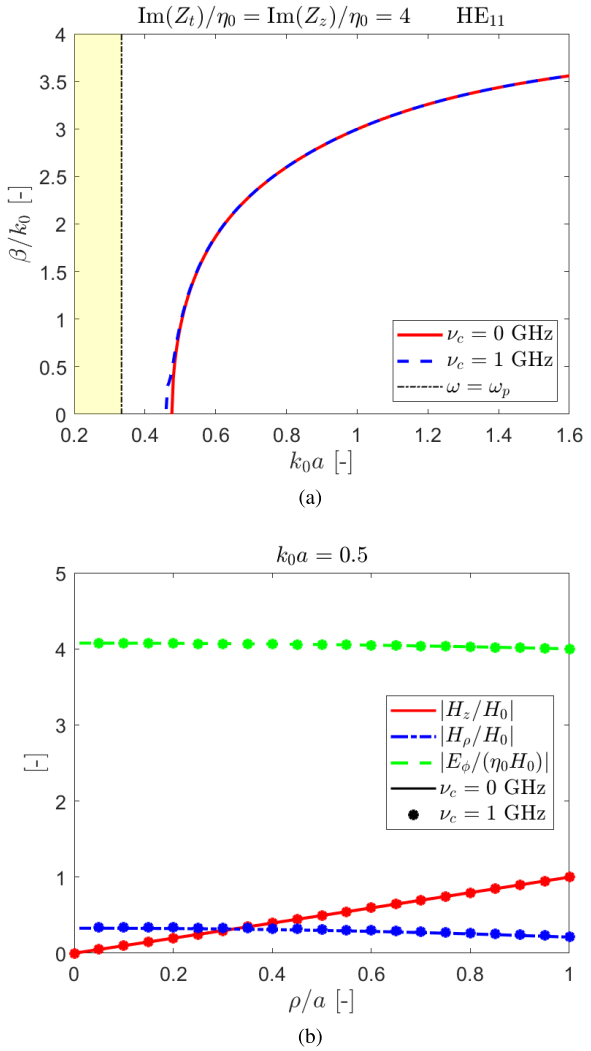

FIGURE 13. (a) Dispersion relation for the mode HE$_{11}$ and (b) normalized EM fields vs. the normalized radial coordinate ρ/a. Comparison between non-collisional ($\nu_c = 0$ GHz) and collisional ($\nu_c = 1$ GHz) plasma. The plasma frequency is assumed such that $a\omega_p/c_0 = 0.33$.

close to a metasurface [65]. As a result, additional verification corroborates the theoretical model discussed in Section II-A even when the surface impedance is anisotropic.

V. CONCLUSION

This work focuses on a metasurface-cladded waveguide that supports EM propagation if loaded with positive and negative-epsilon materials. First, a theoretical model has been discussed to assess the wave modes propagating regimes in the proposed structure. Theoretical results have been verified against numerical predictions. The theoretical findings laid the foundation for the numerical design, which consists of a hollow dielectric substrate enclosed in a metal sheet. The internal surface of the waveguide is coated with a lattice of metallic patches. The filling dielectric and the geometry of the metallic lattice have a major effect on the waveguide propagation regime, particularly on the cut-off frequency. Nonetheless, propagation is demonstrated with both positive and negative-epsilon filling materials. This promotes the proposed design as a microwave device for plasma discharges [2]. Moreover, the possibility of using a metasurface-cladded waveguide as a plasma diagnostic system is worth further investigation, given the dependence of the cut-off frequency from ε_r.

Future work envisions the implementation of a proof of concept to validate the current results. Several strategies can be employed to realize the proposed waveguide. One option utilizes conventional printed circuit board techniques, such as inkjet or screen printing [67]. For this approach, a flexible substrate is required, allowing it to be printed flat and then bent into a cylindrical shape, secured by an external dielectric or metal sheet. The increasing demand for flexible circuits, including sensors and wearables, has led to the use of various organic dielectric materials as substrates [68]. Additionally, metal nanoparticle-based conductive inks are commonly used to create the conductive pattern [69]. Another approach involves technologies capable of producing conductive patterns directly on curved surfaces. Using intense pulsed light-induced mass transfer, patterned circuits have

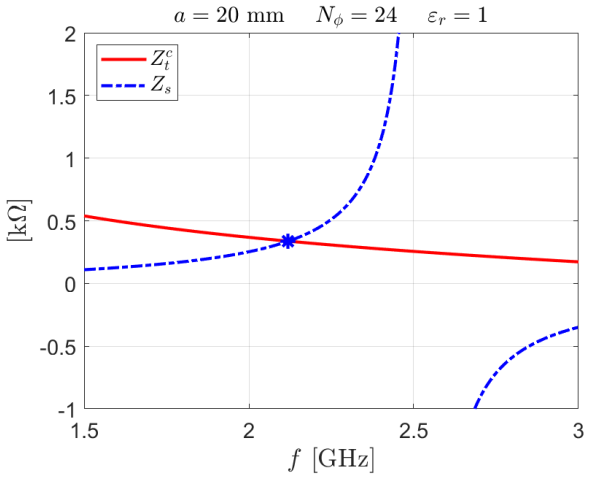

FIGURE 14. Surface impedance Z_s and cut-off impedance Z_t^c associated to the mode HE_{11} in function of the signal frequency.

TABLE 2. Cut-off frequency estimated numerically and theoretically. Operative conditions as in Fig. 14.

N_ϕ	6	8	10	12	16	20	24
f^c_{num} [GHz]	1.2	1.4	1.5	1.6	1.8	2.0	2.1
f^c_{theor} [GHz]	1.1	1.2	1.3	1.4	1.6	1.7	1.8

been fabricated on convex and concave surfaces [70]. In this method, the waveguide is produced in two parts, consisting of two hemicylinders, eliminating the need for a flexible substrate. Instead, any suitable dielectric material can be used, with an external metal sheet ensuring tightness and geometrical precision in the final assembly. Given the need to combine expertise in electromagnetics, material science, and plasma technology, the realization of a proof of concept for the proposed technology will be addressed in a forthcoming paper.

APPENDIX A
PLASMA COLLISIONALITY

The rationale of assuming a non-collisional plasma for the analyses accomplished in Sections III, IV is proven in the following. The case examined via the theoretical model in Section III-B is further investigated by comparing the results obtained with non-collisional ($\nu_c = 0$ GHz) and collisional ($\nu_c = 1$ GHz) plasma in Fig. 13. Notably, the configuration analysed assumes $a = 10$ mm and $\omega_p = 10^{10}$ rad/s, namely it is consistent with the operative conditions of plasma antennas [71]. Results are presented for the mode HE_{11} and positive surface impedance, but they have general validity. Specifically, assuming a collisional plasma mildly affects the resultant axial wavenumber β and EM field profiles. This is consistent with previous results handling EM propagation within plasma if $\nu_c < \omega \approx \omega_p$ [47]. The major effect caused by assuming $\nu_c \neq 0$ is that traveling waves are dumped, their exponential decay is quantified via a dumping coefficient whose value is $\alpha/k_0 = 0.2$ for $k_0 a = 0.5$ and $\nu_c = 1$ GHz. Specifically, the intensity of EM fields is halved at about 100 mm, perfectly consistent with exploiting the proposed configuration in a plasma discharge [2].

APPENDIX B
METASURFACE DISPERSION MODEL

The methodology adopted to interpret the results presented in Section IV-A via the simplified analytical model proposed in [37] is deepened in the following. The cladding metasurface has a dispersive behavior; namely, its surface impedance is not constant with frequency [39]. Simplified analytical models have been proposed to handle plane metasurfaces [37], [59], [62], [63]. Specifically, the formulation presented in [37] has been adopted in this work. Such a model provides preliminary results given that the conformal nature of the cladding metasurface is ignored [64]. For a certain value of N_ϕ, and in turn of D and D_ϕ, the surface impedance offered by the metasurface Z_s is compared against the frequency that triggers cut-off. In the case considered in Fig. 14, namely $\varepsilon_r = 1$ and mode HE_{11}, the cut-off impedance is Z_t^c. The interception between the two curves determines the cut-off frequency f^c. In Table 2, the estimation of f_c via the proposed theoretical methodology is compared against the numerical results presented in Section IV-A. Notably, a maximum disagreement of 15% is found, which is considered acceptable if this approach is adopted to interpret the dynamics of the waveguide qualitatively.

REFERENCES

[1] F. F. Chen, *Introduction to Plasma Physics*. Berlin, Germany: Springer, 2012.
[2] C. M. Ferreira and M. Moisan, *Microwave Discharges: Fundamentals and Applications*, vol. 302. Berlin, Germany: Springer, 2013.
[3] S. J. Pearton, C. R. Abernathy, and F. Ren, "Low bias electron cyclotron resonance plasma etching of GaN, AlN, and InN," *Appl. Phys. Lett.*, vol. 64, no. 17, pp. 2294–2296, Apr. 1994.
[4] M. Manente and M. Magarotto, "Electric propulsion systems," in *Next Generation CubeSats and SmallSats*. Amsterdam, The Netherlands: Elsevier, 2023, ch. 20, pp. 485–517.
[5] F. Cannat, T. Lafleur, J. Jarrige, P. Chabert, P.-Q. Elias, and D. Packan, "Optimization of a coaxial electron cyclotron resonance plasma thruster with an analytical model," *Phys. Plasmas*, vol. 22, no. 5, May 2015, Art. no. 053503.
[6] J. P. Rayner, A. P. Whichello, and A. D. Cheetham, "Physical characteristics of plasma antennas," *IEEE Trans. Plasma Sci.*, vol. 32, no. 1, pp. 269–281, Feb. 2004.
[7] M. Moisan, A. Shivarova, and A. W. Trivelpiece, "Experimental investigations of the propagation of surface waves along a plasma column," *Plasma Phys.*, vol. 24, no. 11, pp. 1331–1400, Nov. 1982.
[8] J. Asmussen, "Electron cyclotron resonance microwave discharges for etching and thin-film deposition," *J. Vac. Sci. Technol. A, Vac., Surf., Films*, vol. 7, no. 3, pp. 883–893, May 1989.
[9] I. Adamovich, S. Baalrud, A. Bogaerts, P. Bruggeman, M. Cappelli, V. Colombo, U. Czarnetzki, U. Ebert, J. G. Eden, and P. Favia, "The 2017 plasma roadmap: Low temperature plasma science and technology," *J. Phys. D, Appl. Phys.*, vol. 50, no. 32, 2017, Art. no. 323001.
[10] I. Adamovich, S. Agarwal, E. Ahedo, L. L. Alves, S. Baalrud, N. Babaeva, A. Bogaerts, A. Bourdon, P. Bruggeman, and C. Canal, "The 2022 plasma roadmap: Low temperature plasma science and technology," *J. Phys. D, Appl. Phys.*, vol. 55, no. 37, p. 373001, Sep. 2022.

[11] M. Magarotto, L. Schenato, P. De Carlo, and A.-D. Capobianco, "Feasibility of a plasma-based intelligent reflective surface," *IEEE Access*, vol. 10, pp. 97995–98003, 2022.

[12] T. Tamir and A. A. Oliner, "The spectrum of electromagnetic waves guided by a plasma layer," *Proc. IEEE*, vol. 51, no. 2, pp. 317–332, 1963.

[13] M. Moisan and Z. Zakrzewski, "Plasma sources based on the propagation of electromagnetic surface waves," *J. Phys. D, Appl. Phys.*, vol. 24, no. 7, pp. 1025–1048, Jul. 1991.

[14] F. F. Chen, "Helicon discharges and sources: A review," *Plasma Sources Sci. Technol.*, vol. 24, no. 1, Jan. 2015, Art. no. 014001.

[15] S. S. S. Shinohara, "Propagating wave characteristics for plasma production in plasma processing field," *Jpn. J. Appl. Phys.*, vol. 36, no. 7S, p. 4695, Jul. 1997.

[16] M. Magarotto, F. Sadeghikia, L. Schenato, D. Rocco, M. Santagiustina, A. Galtarossa, A. K. Horestani, and A.-D. Capobianco, "Plasma antennas: A comprehensive review," *IEEE Access*, vol. 12, pp. 80468–80490, 2024.

[17] C. P. Bates and R. Mittra, "Waveguide excitation of dielectric and plasma slabs," *Radio Sci.*, vol. 3, no. 3, pp. 251–266, Mar. 1968.

[18] S. R. Seshadri and W. F. Pickard, "Surface waves on an anisotropic plasma sheath," *IEEE Trans. Microw. Theory Techn.*, vol. MTT-12, no. 5, pp. 529–541, Sep. 1964.

[19] E. L. Johansen, "The radiation properties of a parallel-plane waveguide in a transversely magnetized, homogeneous plasma," *IEEE Trans. Microw. Theory Techn.*, vol. MTT-13, no. 1, pp. 77–83, Jan. 1965.

[20] T. Kashiwa, N. Yoshida, and I. Fukai, "Transient analysis of a magnetized plasma in three-dimensional space," *IEEE Trans. Antennas Propag.*, vol. AP-36, no. 8, pp. 1096–1105, Aug. 1988.

[21] F. Hunsberger, R. Luebbers, and K. Kunz, "Finite-difference time-domain analysis of gyrotropic media. I. magnetized plasma," *IEEE Trans. Antennas Propag.*, vol. 40, no. 12, pp. 1489–1495, Aug. 1992.

[22] Y. Mouzouris and J. E. Scharer, "Modeling of profile effects for inductive helicon plasma sources," *IEEE Trans. Plasma Sci.*, vol. 24, no. 1, pp. 152–160, Aug. 1996.

[23] M. Magarotto, D. Melazzi, and D. Pavarin, "3D-VIRTUS: Equilibrium condition solver of radio-frequency magnetized plasma discharges for space applications," *Comput. Phys. Commun.*, vol. 247, Feb. 2020, Art. no. 106953.

[24] G. A. Kyriacou, "Wiener-Hopf analysis of planar canonical structures loaded with longitudinally magnetized plasma biased normally to the extra-ordinary wave propagation," *Prog. Electromagn. Res. B*, vol. 5, pp. 1–34, 2008.

[25] X. M. Mitsalas, T. Kaifas, and G. A. Kyriacou, "Wiener-Hopf analysis of planar canonical structures loaded with longitudinally magnetized plasma biased normally to the extraordinary wave propagation: Near and far field," *Prog. Electromagn. Res. B*, vol. 88, pp. 119–149, 2020.

[26] J. G. Pollock and A. K. Iyer, "Below-cutoff propagation in metamaterial-lined circular waveguides," *IEEE Trans. Microw. Theory Techn.*, vol. 61, no. 9, pp. 3169–3178, Sep. 2013.

[27] A. Alu and N. Engheta, "Guided modes in a waveguide filled with a pair of single-negative (SNG), double-negative (DNG), and/or double-positive (DPS) layers," *IEEE Trans. Microw. Theory Techn.*, vol. 52, no. 1, pp. 199–210, Jan. 2004.

[28] J. G. Pollock and A. K. Iyer, "Miniaturized circular-waveguide probe antennas using metamaterial liners," *IEEE Trans. Antennas Propag.*, vol. 63, no. 1, pp. 428–433, Jan. 2015.

[29] X. Wu, C. Hu, M. Wang, M. Pu, and X. Luo, "Realization of low-scattering metamaterial shell based on cylindrical wave expanding theory," *Opt. Exp.*, vol. 23, no. 8, p. 10396, 2015.

[30] J. G. Pollock and A. K. Iyer, "Experimental verification of below-cutoff propagation in miniaturized circular waveguides using anisotropic ENNZ metamaterial liners," *IEEE Trans. Microw. Theory Techn.*, vol. 64, no. 4, pp. 1297–1305, Apr. 2016.

[31] S. Hrabar, J. Bartolic, and Z. Sipus, "Waveguide miniaturization using uniaxial negative permeability metamaterial," *IEEE Trans. Antennas Propag.*, vol. 53, no. 1, pp. 110–119, Jan. 2005.

[32] F.-Y. Meng, Q. Wu, D. Erni, and L.-W. Li, "Controllable metamaterial-loaded waveguides supporting backward and forward waves," *IEEE Trans. Antennas Propag.*, vol. 59, no. 9, pp. 3400–3411, Sep. 2011.

[33] J. G. Pollock, A. K. Iyer, D. Pratap, and S. Anantha Ramakrishna, "A class of circular waveguiding structures containing cylindrically anisotropic metamaterials: Applications from radio frequency/microwave to optical frequencies," *J. Appl. Phys.*, vol. 119, no. 8, Feb. 2016, Art. no. 083103.

[34] N. Raveu, B. Byrne, L. Claudepierre, and N. Capet, "Modal theory for waveguides with anisotropic surface impedance boundaries," *IEEE Trans. Microw. Theory Techn.*, vol. 64, no. 4, pp. 1153–1162, Apr. 2016.

[35] A. Li, S. Singh, and D. Sievenpiper, "Metasurfaces and their applications," *Nanophotonics*, vol. 7, no. 6, pp. 989–1011, Jun. 2018.

[36] H.-T. Chen, A. J. Taylor, and N. Yu, "A review of metasurfaces: Physics and applications," *Rep. Prog. Phys.*, vol. 79, no. 7, Jul. 2016, Art. no. 076401.

[37] D. Sievenpiper, L. Zhang, R. F. J. Broas, N. G. Alexopolous, and E. Yablonovitch, "High-impedance electromagnetic surfaces with a forbidden frequency band," *IEEE Trans. Microw. Theory Techn.*, vol. 47, no. 11, pp. 2059–2074, Nov. 1999.

[38] C. J. Barker, N. De Zanche, and A. K. Iyer, "Dispersion and polarization control in below-cutoff circular waveguides using anisotropic metasurface liners," *IEEE Trans. Microw. Theory Techn.*, vol. 71, no. 8, pp. 3392–3403, Aug. 2023.

[39] M. Magarotto, L. Schenato, G. Franchin, M. Santagiustina, A. Galtarossa, and A.-D. Capobianco, "Cylindrical waveguides for microwave spoof surface plasmon polaritons," *IEEE Access*, vol. 12, pp. 23190–23199, 2024.

[40] L. Kuhler, G. Le Fur, L. Duchesne, and N. Raveu, "The propagation characteristics of 2-D metamaterial waveguides using the modal expansion theory," *IEEE Trans. Microw. Theory Techn.*, vol. 66, no. 10, pp. 4319–4326, Oct. 2018.

[41] O. Luukkonen, C. R. Simovski, A. V. Raisanen, and S. A. Tretyakov, "An efficient and simple analytical model for analysis of propagation properties in impedance waveguides," *IEEE Trans. Microw. Theory Techn.*, vol. 56, no. 7, pp. 1624–1632, Jul. 2008.

[42] Z. Luo, T. J. Cui, and H. F. Ma, "Cutoff manipulation of anisotropic reactance lining in circular waveguides," *Int. J. Microw. Wireless Technol.*, vol. 11, no. 4, pp. 334–340, May 2019.

[43] F.-R. Yang, K.-P. Ma, Y. Qian, and T. Itoh, "A novel TEM waveguide using uniplanar compact photonic-bandgap (UC-PBG) structure," *IEEE Trans. Microw. Theory Techn.*, vol. 47, no. 11, pp. 2092–2098, Nov. 1999.

[44] M. N. M. Kehn, M. Nannetti, A. Cucini, S. Maci, and P.-S. Kildal, "Analysis of dispersion in dipole-FSS loaded hard rectangular waveguide," *IEEE Trans. Antennas Propag.*, vol. 54, no. 12, pp. 2275–2282, Aug. 2006.

[45] I. H. Hutchinson, "Principles of plasma diagnostics," *Plasma Phys. Control. Fusion*, vol. 44, no. 12, p. 2603, 2002.

[46] N. Cselyuszka, Z. Sakotic, V. Crnojevic-Bengin, V. Radonic, and N. Jankovic, "Microwave surface plasmon polariton-like sensor based on half-mode substrate integrated waveguide for highly sensitive dielectric constant detection," *IEEE Sensors J.*, vol. 18, no. 24, pp. 9984–9992, Dec. 2018.

[47] F. F. Chen and D. Arnush, "Generalized theory of helicon waves. I. Normal modes," *Phys. Plasmas*, vol. 4, no. 9, pp. 3411–3421, Sep. 1997.

[48] E. Kelebekler, "Complex surface wave modes of plasma column loaded closed cylindrical waveguide," *Prog. Electromagn. Res. B*, vol. 54, pp. 357–383, 2013.

[49] V. I. Shcherbinin, B. A. Kochetov, A. V. Hlushchenko, and V. I. Tkachenko, "Cutoff frequencies of a dielectric-loaded rectangular waveguide with arbitrary anisotropic surface impedance," *IEEE Trans. Microw. Theory Techn.*, vol. 67, no. 2, pp. 577–583, Feb. 2019.

[50] D. M. Pozar, *Microwave Engineering*. Hoboken, NJ, USA: Wiley, 2011.

[51] D. G. Swanson, *Plasma Waves*. Amsterdam, The Netherlands: Elsevier, 2012.

[52] J. J. Rushchitsky and S. V. Sinchilo, "Variant of the nonlinear wave equations describing cylindrical axisymmetrical waves," *Int. Appl. Mech.*, vol. 54, no. 4, pp. 393–398, Jul. 2018.

[53] K. Y. Kim, "Guided and leaky modes of circular open electromagnetic waveguides: Dielectric, plasma, and metamaterial columns," Ph.D. dissertation, Dept. Electron., Kyungpook Nat. Univ., Daegu, South Korea, 2004.

[54] R. R. Hirani, S. K. Pathak, S. N. Shah, and D. K. Sharma, "Dispersion characteristics of dielectric tube waveguide loaded with plasma for leaky wave antenna application," *AEU Int. J. Electron. Commun.*, vol. 83, pp. 123–130, Jan. 2018.

[55] B. M. Thomas and H. C. Minnett, "Modes of propagation in cylindrical waveguides with anisotropic walls," *Proc. Inst. Electr. Engineers*, vol. 125, no. 10, p. 929, 1978.

[56] T. Abe and Y. Yamaguchi, "Propagation constant below cutoff frequency in a circular waveguide with conducting medium," *IEEE Trans. Microw. Theory Techn.*, vol. MTT-29, no. 7, pp. 707–712, Jul. 1981.

[57] S. F. Mahmoud, *Electromagnetic Waveguides: Theory and Applications*, no. 32. London, U.K.: IET, 1991.

[58] L. Kuhler, N. Raveu, G. Le Fur, and L. Duchesne, "The modal expansion theory applied to 3-D metamaterial waveguides characterization," *Prog. Electromagn. Res. M*, vol. 92, pp. 31–41, 2020.
[59] M. Borgese and F. Costa, "A simple equivalent circuit approach for anisotropic frequency-selective surfaces and metasurfaces," *IEEE Trans. Antennas Propag.*, vol. 68, no. 10, pp. 7088–7098, Oct. 2020.
[60] R. R. Hirani, S. K. Pathak, and S. N. Shah, "Full-wave analysis and computation of radiation characteristics for reconfigurable plasma antennas," *IEEE Trans. Antennas Propag.*, vol. 67, no. 8, pp. 5185–5193, Aug. 2019.
[61] *Rogers Corporation Website*. Accessed: Nov. 13, 2023. [Online]. Available: https://www.rogerscorp.com/advanced-electronics-solutions/rt-duroid-laminates
[62] A. B. Yakovlev, O. Luukkonen, C. R. Simovski, S. A. Tretyakov, S. Paulotto, P. Baccarelli, and G. W. Hanson, "Analytical modeling of surface waves on high impedance surfaces," in *Metamaterials and Plasmonics: Fundamentals, Modelling, Applications*. Dordrecht, The Netherlands: Springer, 2009, pp. 239–254.
[63] A. M. Patel and A. Grbic, "Modeling and analysis of printed-circuit tensor impedance surfaces," *IEEE Trans. Antennas Propag.*, vol. 61, no. 1, pp. 211–220, Jan. 2013.
[64] L. La Spada, C. Spooner, S. Haq, and Y. Hao, "Curvilinear MetaSurfaces for surface wave manipulation," *Sci. Rep.*, vol. 9, no. 1, p. 3107, Feb. 2019.
[65] D. R. Smith and J. B. Pendry, "Homogenization of metamaterials by field averaging," *J. Opt. Soc. Amer. B, Opt. Phys.*, vol. 23, no. 3, pp. 391–403, 2006.
[66] A. Alù, "First-principles homogenization theory for periodic metamaterials," *Phys. Rev. B, Condens. Matter*, vol. 84, no. 7, Aug. 2011, Art. no. 075153.
[67] P. He, J. Cao, H. Ding, C. Liu, J. Neilson, Z. Li, I. A. Kinloch, and B. Derby, "Screen-printing of a highly conductive graphene ink for flexible printed electronics," *ACS Appl. Mater. Interfaces*, vol. 11, no. 35, pp. 32225–32234, Sep. 2019.
[68] Z. Li, S. K. Sinha, G. M. Treich, Y. Wang, Q. Yang, A. A. Deshmukh, G. A. Sotzing, and Y. Cao, "All-organic flexible fabric antenna for wearable electronics," *J. Mater. Chem. C*, vol. 8, no. 17, pp. 5662–5667, 2020.
[69] S. G. Kirtania, A. W. Elger, M. R. Hasan, A. Wisniewska, K. Sekhar, T. Karacolak, and P. K. Sekhar, "Flexible antennas: A review," *Micromachines*, vol. 11, no. 9, p. 847, Sep. 2020.
[70] N. Yi, Y. Gao, A. Lo Verso, J. Zhu, D. Erdely, C. Xue, R. Lavelle, and H. Cheng, "Fabricating functional circuits on 3D freeform surfaces via intense pulsed light-induced zinc mass transfer," *Mater. Today*, vol. 50, pp. 24–34, Nov. 2021.
[71] M. Magarotto, L. Schenato, M. Santagiustina, A. Galtarossa, and A.-D. Capobianco, "Plasma-based intelligent reflecting surface for beam-steering and polarization conversion," *IEEE Access*, vol. 11, pp. 43546–43556, 2023.

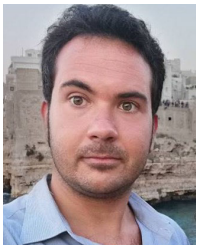

MIRKO MAGAROTTO (Member, IEEE) received the M.Sc. degree in aerospace engineering and the Ph.D. degree in science technology and measurements for space from the University of Padova, Padua, Italy, in 2015 and 2019, respectively. He is an Assistant Professor (RTDa) with the Department of Information Engineering, University of Padova. His current research interests include plasma antennas, plasma numerical simulation, and electric space propulsion.

LUCA SCHENATO (Member, IEEE) received the M.Sc. degree in telecommunication engineering and the Ph.D. degree in electronic and telecommunication engineering from the University of Padova, Padua, Italy, in 2003 and 2007, respectively. He is an Assistant Professor (RTDb) with the Department of Information Engineering, University of Padova. His research interests include optical fiber sensors, optical fiber-based devices, and intelligent reflective surfaces.

MARCO SANTAGIUSTINA (Member, IEEE) received the M.Sc. degree in electronic engineering and the Ph.D. degree in electronic and telecommunication engineering from the University of Padova, Padua, Italy, in 1992 and 1996, respectively. He is a Full Professor with the Department of Information Engineering, University of Padova. His current research interests include nonlinear optics, optical fibers, and electromagnetic field theory.

ANDREA GALTAROSSA (Life Fellow, IEEE) is a Full Professor of electromagnetic waves and photonics with the Department of Information Engineering, University of Padova, Italy. He has co-authored more than 200 papers in journals and conference proceedings. His research interests include optical fiber design, distributed characterization of single-mode and special fibers, and distributed sensing. He is a fellow of OPTICA. He has been a member of the Technical Program Committee for the European Conference on Optical Communication (ECOC) and the Optical Fiber Communication Conference (OFC). He has been the Topical Editor and the Deputy Editor of *Optics Letters*.

ANTONIO-DANIELE CAPOBIANCO (Member, IEEE) received the M.Sc. degree in electronic engineering and the Ph.D. degree in electronic and telecommunication engineering from the University of Padova, Padua, Italy, in 1989 and 1994, respectively. He is an Associate Professor with the Department of Information Engineering, University of Padova. His current research interests include theory and numerical modeling in photonics, plasmonics, and microwave antennas.

Open Access funding provided by 'Università degli Studi di Padova' within the CRUI CARE Agreement